

Title	Germanium nanowire synthesis from fluorothiolate-capped gold nanoparticles in supercritical carbon dioxide
Authors	Collins, Gillian;Kolešnik-Gray, Maria M.;Krstić, Vojislav;Holmes, Justin D.
Publication date	2010-08-20
Original Citation	Collins, G., Kolešnik, M., Krstić, V. and Holmes, J. D. (2010) 'Germanium Nanowire Synthesis from Fluorothiolate-Capped Gold Nanoparticles in Supercritical Carbon Dioxide', Chemistry of Materials, 22(18), pp. 5235-5243. doi: 10.1021/cm1012137
Type of publication	Article (peer-reviewed)
Link to publisher's version	http://pubs.acs.org/doi/abs/10.1021/cm1012137 - 10.1021/cm1012137
Rights	© 2010 American Chemical Society. This document is the Accepted Manuscript version of a Published Work that appeared in final form in Chemistry of Materials, copyright © American Chemical Society after peer review and technical editing by the publisher. To access the final edited and published work see http://pubs.acs.org/doi/abs/10.1021/cm1012137
Download date	2025-06-06 17:14:24
Item downloaded from	https://hdl.handle.net/10468/6688



UCC

University College Cork, Ireland
Coláiste na hOllscoile Corcaigh

Germanium Nanowire Synthesis from Fluorothiolate-Capped Gold Nanoparticles in Supercritical Carbon Dioxide

Gillian Collins^{1,2}, Maria Kolečnik^{2,3}, Vojislav Krstić^{2,3} and Justin D. Holmes^{1,2}*

¹Materials and Supercritical Fluids Group, Department of Chemistry and the Tyndall National Institute, University College Cork, Cork, Ireland. ²Centre for Research on Adaptive Nanostructures and Nanodevices (CRANN), Trinity College Dublin, Dublin 2, Ireland. ³School of Physics, Trinity College Dublin, Dublin 2, Ireland.

*To whom correspondence should be addressed: Tel: +353(0)21 4903608; Fax: +353 (0)21 4274097; E-mail: j.holmes@ucc.ie

Abstract

Ge nanowires seeded from Au nanoparticles capped with fluorothiolate ligands were synthesized in supercritical carbon dioxide (sc-CO₂) by the thermal decomposition of diphenylgermane (DPG) at a temperature of 380 °C and a pressure of 25.7 MPa. Both perfluorinated and semi-fluorinated capped Au nanoparticles acted as effective catalysts for growing Ge nanowires, with mean diameters of 11 nm ($\sigma = 2.8$) and 14 nm ($\sigma = 3.5$), respectively. The mean diameter of Ge nanowires grown from the fluorous-capped Au nanoparticles were considerably smaller than those synthesized from dodecanethiol-capped nanoparticles in sc-toluene, under the same reaction conditions, *i.e.* 28 nm, $\sigma = 10.3$. Differences in the ligand conformations on the surface of the Au nanoparticles and phase separation of the fluorocarbon/CO₂ and hydrocarbon/toluene systems, gave rise to greater steric stabilisation of

the fluorine-capped Au nanoparticles in CO₂, resulting in small diameter nanowires with a relatively narrow size distribution. Electrical analysis of the nanowires showed them to be *p*-type (hole) semiconductors.

Introduction

In recent years, extensive research has focused on the synthesis, assembly and potential applications of Group IV semiconductor nanowires, due to their size-dependent electrical, optical and mechanical properties that are not observed in the bulk materials¹⁻⁶. There is particular interest in the controlled synthesis of nanowires below their Bohr radius, where quantum confinement effects become prominent⁷. Germanium (Ge) possesses a considerably larger Bohr radius compared to silicon (Si), *i.e.* 24.3 nm and 4.9 nm respectively; however diameter control at this length scale is lacking. Templated structures such as ordered mesoporous silicates and anodic aluminium oxide (AAO) allow good control over nanowire diameters but templating techniques often produce poorly crystalline nanowires and complete filling of small-pore templates has proved difficult⁸⁻⁹. Patterning of substrates with Au nanoparticles by lithographic techniques, or the use of colloidal nanoparticles, have proved an effective route for the controlled growth of Ge nanowires in the diameter range between 20-50 nm¹⁰⁻¹². Colloid-mediated growth has been applied to the vapour-liquid-solid (VLS), solution-liquid-solid (SLS) and supercritical fluid-liquid-solid (SFLS) synthesis of Ge nanowires¹³⁻¹⁵. The synthesis of high yields of small diameter nanowires (< 20 nm) with narrow size distributions remains challenging as Au nanoparticles readily aggregate when subjected to elevated synthesis temperatures, particularly if the concentration of nanoparticles is high. Solution synthesis of Ge nanowires seeded from organic monolayer capped Au nanoparticles dispersed in supercritical (sc) organic solvents, has previously been shown to produce high quality crystalline nanowires¹⁶⁻¹⁷. Furthermore, the ability to solubilise a greater concentration of precursor relative to vapour phase techniques can result in nanowire yields of milligram quantities¹⁷⁻¹⁸. Korgel *et al.*¹⁹⁻²⁰ reported that Ni-seeded Ge nanowires grown in sc-toluene had a mean diameter of 14.5 nm compared to Au-seeded nanowires, which had a mean diameter of 55 nm. This reduction in the mean nanowire

diameter was attributed to a solid-phase growth mechanism where the solid Ni-Ge eutectic droplet is less susceptible to aggregation compared to Au, which forms a liquid alloyed seed droplet¹³.

Extending the supercritical fluid (SCF) approach to nanowire synthesis we investigate supercritical carbon dioxide (sc-CO₂) as a solvent for Ge nanowire growth. CO₂ is among the most widely used SCF having relatively low critical conditions ($T_c = 31\text{ }^{\circ}\text{C}$, $P_c = 7.4\text{ MPa}$) and additionally it is non-flammable, non-toxic and an environmentally friendly solvent, making it an attractive alternative to conventional organic solvents²¹. CO₂ also offers significant challenges as a solvent; its low polarizability per volume and low dielectric constant results in weaker van der Waals forces compared to hydrocarbon solvents²²⁻²³. While CO₂ can solubilize some low molecular weight hydrocarbons, it is a poor solvent for most non-volatile lipophilic and hydrophilic solutes²⁴. One strategy for overcoming these solvation problems is to use ‘CO₂-philic’ ligands such as fluorinated compounds. Fluorocarbons display high solubility in CO₂ owing to their low cohesive energy densities which provide favorable energetic interactions with the solvent²⁵. Harrison *et al.*²⁶ were the first to report the formation of water-in-CO₂ micromulsions by the use of hybrid fluorocarbon-hydrocarbon surfactants. Fluorocarbon-coated Ag, Pt and Ir nanoparticles have also been synthesized in sc-CO₂ by arrested precipitation, where the tunable solvent density of CO₂ allowed the dimensions of the nanoparticles to be tailored²⁷⁻²⁸.

The origin of the high solubility of fluorocarbons in CO₂ has been the subject of many theoretical and experimental investigations; however considerable debate still remains regarding the specific nature of fluorocarbon-CO₂ interactions. Using NMR Dardin *et al.*²⁹ found differences in the chemical shifts of ¹H and ¹⁹F nuclei, suggesting the presence of a specific fluorocarbon-CO₂ interaction. Later NMR studies and molecular dynamics simulations carried out by Yonker *et al.*³⁰⁻³¹, found no evidence for a distinct fluorine-CO₂ interaction. Wallen³² reported that the interactions of hydrocarbons and fluorocarbons with CO₂ while energetically comparable are fundamentally

different in nature, with fluorocarbons interacting through the carbon atom of CO₂ and hydrocarbons interacting through the oxygen atoms.

Here we report the synthesis of Au nanoparticles stabilized by perfluorinated and semi-fluorinated ligands and their use as catalysts for the growth of Ge nanowires in sc-CO₂. We investigate the effect of the fluorine-capped Au catalysts on the growth of Ge nanowires, compared to those seeded from hydrocarbon-capped Au nanoparticles grown in supercritical hydrocarbon solvents.

Experimental

Au Nanoparticle Synthesis

1H, 1H, 2H, 2H perfluorodecanethiol, 6-(perfluorohexyl)hexanol and perfluorohexane were purchased for ABCR GmbH & Co. KG, Germany. All other chemicals were purchased from Sigma Aldrich. The semi-fluorinated thiol was synthesized from the corresponding alcohol using modified literature procedures³³⁻³⁴. Briefly, the alcohol and PPh₃ were dissolved in dry acetonitrile in a 2-neck round bottom flask with a condenser attached. The flask was degassed with N₂ and heated to 70 °C. At this temperature bromine was added dropwise under constant stirring. The reaction proceeded for 6 hr. The bromide was extracted with ether, washed three times with saturated NaCl solution, dried over anhydrous MgSO₄ and the solvent removed on a rotary evaporator. IR (KBr, cm⁻¹) 2920-2860 (ν_{CH}), 1240-1145 (ν_{CF}), 566 (ν_{CBr}).

The bromide was converted to the thiol via a thioacetate derivative using thioacetic acid. Briefly, a freshly prepared sodium methoxide solution was cooled in an ice bath and thioacetic acid was added dropwise, followed by the bromide. The mixture was heated to 70 °C and left to stir for 6 h. The thioacetate derivative was extracted by the procedure previously described. The thiol was obtained by refluxing the thioacetate derivative in NaOH under nitrogen. The thiol was recovered by extraction with ether, washed three times with saturated NaCl solution, dried over anhydrous MgSO₄ and the solvent removed. IR (KBr, cm⁻¹) 2930-2860 (ν_{CH}), 2580 (ν_{SH}), 1240-1145 (ν_{CF}). ¹H NMR,

CDCl₃, 298 K. δ 1.4 (m, 13H, (CH₂)₆ and SH); 1.5 (m, 4H, CH₂CH₂CF₂ and 2H, CH₂CH₂SH); 1.9 (m, 2H, CH₂CF₂); 2.5 (td, 2H, CH₂SH, J = 7.3 Hz).

Au nanoparticles stabilized by dodecanethiol (DDT), 1H, 1H, 2H, 2H perfluorodecanethiol (pF), and 6-(perfluorohexyl)hexane thiol (semi-F) were synthesized based on the Brust method³⁵⁻³⁶. Au nanoparticles were isolated as black solids and dried in a vacuum oven overnight. The dried products were weighed correct to 5 decimal places. Thermal gravimetric analysis (TGA) of the capped Au nanoparticles was used to determine the organic weight fraction, thereby allowing accurate Au concentrations to be used for the synthesis of the Ge nanowires. The fluorine-capped nanoparticles were dispersed in perfluorohexane and the dodecanethiol capped nanoparticles were dispersed in toluene.

Ge Nanowire Synthesis in sc-CO₂

Ge nanowires were synthesized by thermal degradation of an organo-germane precursor in the presence of thiolate-capped Au nanoparticles. Details of the SCF experimental set-up have been described elsewhere^{16, 37}. Ge nanowires were synthesized using two procedures, an injection method and by batch reaction. Injection method: for the fluorothiolate capped Au nanoparticles-CO₂ system, the Ge precursor, diphenylgermane (DPG), and Au nanoparticles, dissolved in a minimum amount of perfluorohexane (Au:Ge molar ratio of 1:1000), were loaded into an injection cell under a nitrogen atmosphere. The injection cell was pressurized to 27.6 MPa. A second reaction cell, containing a Si wafer sealed under a nitrogen atmosphere, was then heated to 380 °C and pressurized to 27.6 MPa. The Si wafer provided a substrate to collect the reaction product. The precursor solution was injected via an injection loop into the reaction cell and the reaction proceeded for 40 min. The cell was cooled to room temperature and slowly depressurized. The DDT-Au nanoparticle/toluene system followed the same reaction procedure. Each reaction was repeated three times in order to observe accurate trends in nanowire diameters and distributions. Statistical data determining

nanowire diameters and size distributions were based on the analysis of at least 150 nanowires for each synthesis.

Materials Characterization

Au nanoparticles and Ge nanowires were characterized using scanning electron microscopy (SEM), transmission electron microscopy (TEM), X-ray diffraction (XRD), thermogravimetric analysis (TGA) and infrared (IR) spectroscopy. SEM images were acquired on a FEI Inspect F instrument, operating at a 5 kV accelerating voltage. TEM images were acquired using a Jeol 2000 FX and Jeol 2100 at 200 kV accelerating voltage. X-Ray diffraction (XRD) measurements were carried out using a Philips X'Pert Data Collector. TGA was performed on a TA Instruments Q500 TGA, using ~20 mg of Au nanoparticles weighed onto a Pt dish. The experiments were run from 25-450 °C at a heating rate of 5 °C min⁻¹ in air. IR spectra were recorded on a BioRad FTS-40A FTIR spectrometer. Spectra were measured at a resolution of 4 cm⁻¹. XPS data was also acquired using a KRATOS AXIS 165 X-ray photoelectron spectrometer equipped with a dual anode (Mg/Al) source. Survey spectra were captured at a pass energy of 100 eV, step size 1 eV and dwell time of 50 ms. The core level spectra were an average of 10 scans captured at a PE of 25 eV, step size of 0.05 eV and dwell time of 100 ms.

For the electrical characterization of individual germanium nanowires, the nanowire raw material was first dispersed in isopropanol and then single nanowires were deposited by drop-casting on a thermally grown SiO₂ layer (thickness 300 nm) on top of a highly doped Si-wafer (serves as back-gate). On the substrate a marker system was predefined allowing for the selectively addressing of individual wires for the following electrical contacting procedure. Single tubes were contacted by standard electron-beam lithography and subsequent metal deposition process. DC electrical measurements on single nanowires were carried out under ambient conditions at room temperature.

Results and Discussion

Nanoparticle Synthesis and Characterization

Figures 1 (a)-(c) show TEM images of Au nanoparticles capped by perfluorodecanethiol (pF), (perfluorohexyl)hexane thiol (semi-F) and dodecanethiol (DDT) ligands, respectively. The fluororous-capped nanoparticles were non-dispersible in common organic solvents, such as toluene, chloroform or acetone, but could be dispersed in fluorinated solvents such as perfluorohexane. Size selective precipitation was undertaken to produce capped Au nanoparticles with mean diameters close to 2 nm and with a polydispersity not more than 20 %. The mean diameters were 2.1 nm ($\sigma = 0.29$), 2.3 nm ($\sigma = 0.46$) and 2.2 nm ($\sigma = 0.33$) for the pF, semi-F and DDT-capped Au nanoparticles, respectively.

FTIR spectroscopy of the Au-capped nanoparticles, shown in figure 2, confirmed the presence of fluorinated ligands on the surface of the nanoparticles. Absorption peaks located at 1205 cm^{-1} and 1240 cm^{-1} could be assigned to the asymmetric stretch (ν_a) of the CF_2 group and the band located at 1145 cm^{-1} could be attributed to the symmetric (ν_s) CF_2 stretch³⁸. XPS was carried out to confirm the attachment of the thiol capping ligands to the Au nanoparticles. Figure 3(a) illustrates the S $2p$ doublet from the pF-Au and semiF-Au nanoparticles. The S $2p_{3/2}$ peak was located at a binding energy of 162.2 eV for both samples, which is in excellent agreement with literature reports for bound thiolates on Au surfaces³⁹⁻⁴¹. The absence of a S $2p_{3/2}$ peak at 163 eV indicates that free thiols *i.e.* unbound thiols, are not present⁴¹. Furthermore, the C $1s$ spectra, shown in figure 3(b) confirms the presence and chemical composition of the perfluorinated and semi-fluorinated ligands. Fluorocarbons give rise to large chemical shifts in the C $1s$ spectra, which are clearly observed at binding energies of 291.1 eV and 293.5 eV, corresponding to the CF_2 and CF_3 functionalities, respectively⁴². The greater intensity of the aliphatic hydrocarbon peak (285 eV) of the semi-F Au nanoparticles compared to the pF-Au nanoparticles is consistent with the larger hydrocarbon component present in the semi-fluorinated capping ligands.

Figure 2(b) shows the TGA weight loss profiles for the Au nanoparticles. The DDT and semi-F ligands displayed a smooth desorption from the surface of the nanoparticles, while the pF-capped nanoparticles show a two step weight loss, which has been attributed to the lower volatility of the hydrocarbon ligand⁴³. The organic weight fraction of the capping ligands was found to be 47, 39 and 27 %, corresponding to *ca.* 102, 118 and 108 ligands per nanoparticle for the pF, semi-F and DDT ligands, respectively. The ligand grafting density was estimated from the mean diameters of the nanoparticles obtained from TEM analysis; the polydispersity of the nanoparticles was not taken into account.

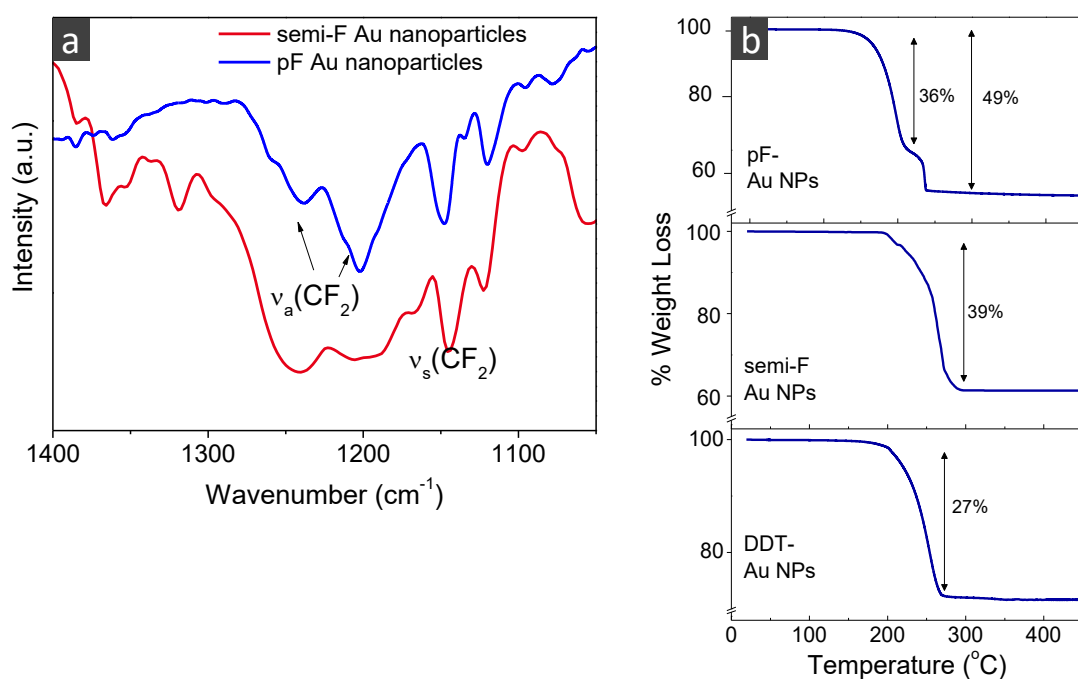


Figure 2. (a) FTIR of fluorinated-capped Au nanoparticles and (b) TGA weight loss profile for fluorinated-capped and DDT- capped Au nanoparticles.

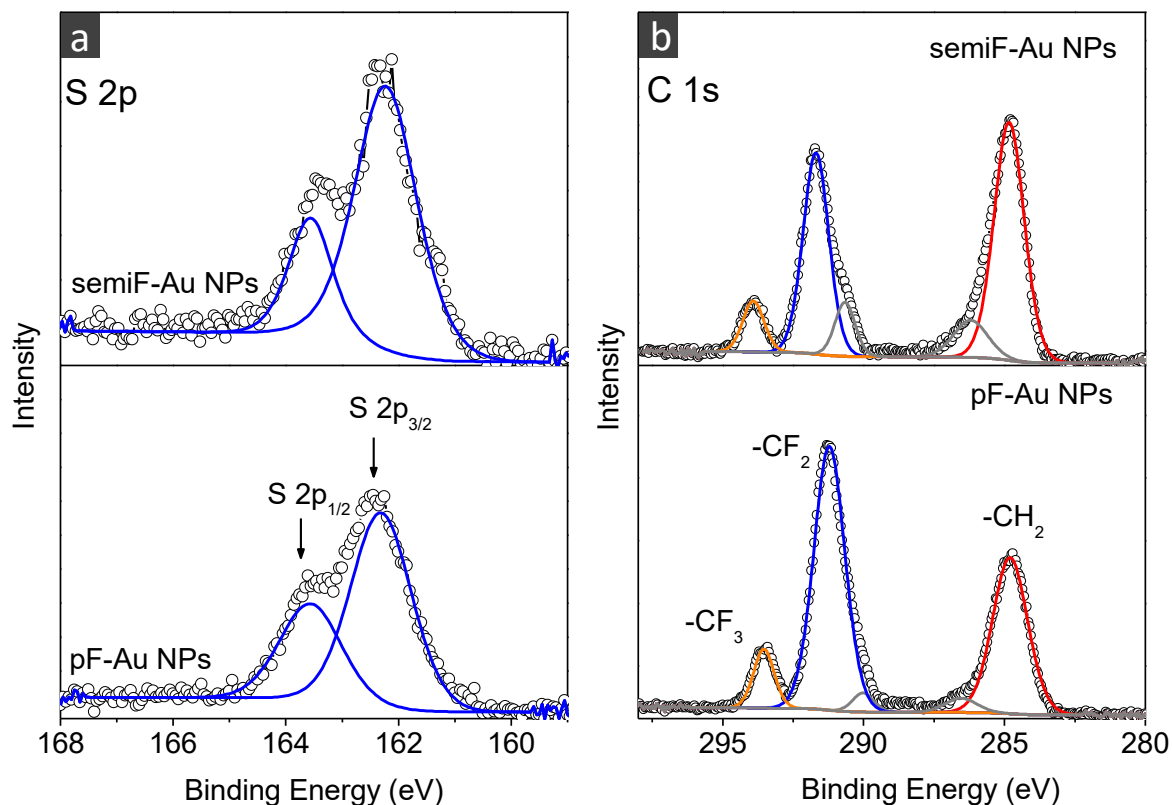


Figure 3. XPS data showing (a) S 2p and (b) C 1s XP spectra of pF-Au and semiF-Au nanoparticles.

Ge Nanowire Synthesis in sc-CO₂

Ge nanowires were synthesized from Au nanoparticles stabilized by three different capping ligands; DDT in sc-toluene and pF and semi-F both in sc-CO₂. Figure 4 shows SEM images and diameter distributions of Ge nanowires synthesized at 380 °C and 27.6 MPa. The pF-capped nanoparticles produced Ge nanowires with the smallest mean diameter (D_{avg}) of 11 nm and standard deviation, $\sigma = 2.8$ (relative error over 3 experiments = 12 %). In comparison, Ge nanowires grown from DDT-capped Au nanoparticles in sc-toluene had a $D_{\text{avg}} = 28$ nm and were substantially more polydisperse ($\sigma = 10.5$). The semi-F ligands, which contain a significant hydrocarbon component (F₆H₆) yielded nanowires with $D_{\text{avg}} = 14$ nm ($\sigma = 3.5$, relative error over 3 experiments = 21 %). The XRD patterns, figure 4(e), of the all of the nanowires synthesized in this study could be indexed to crystalline Ge with a diamond cubic structure.

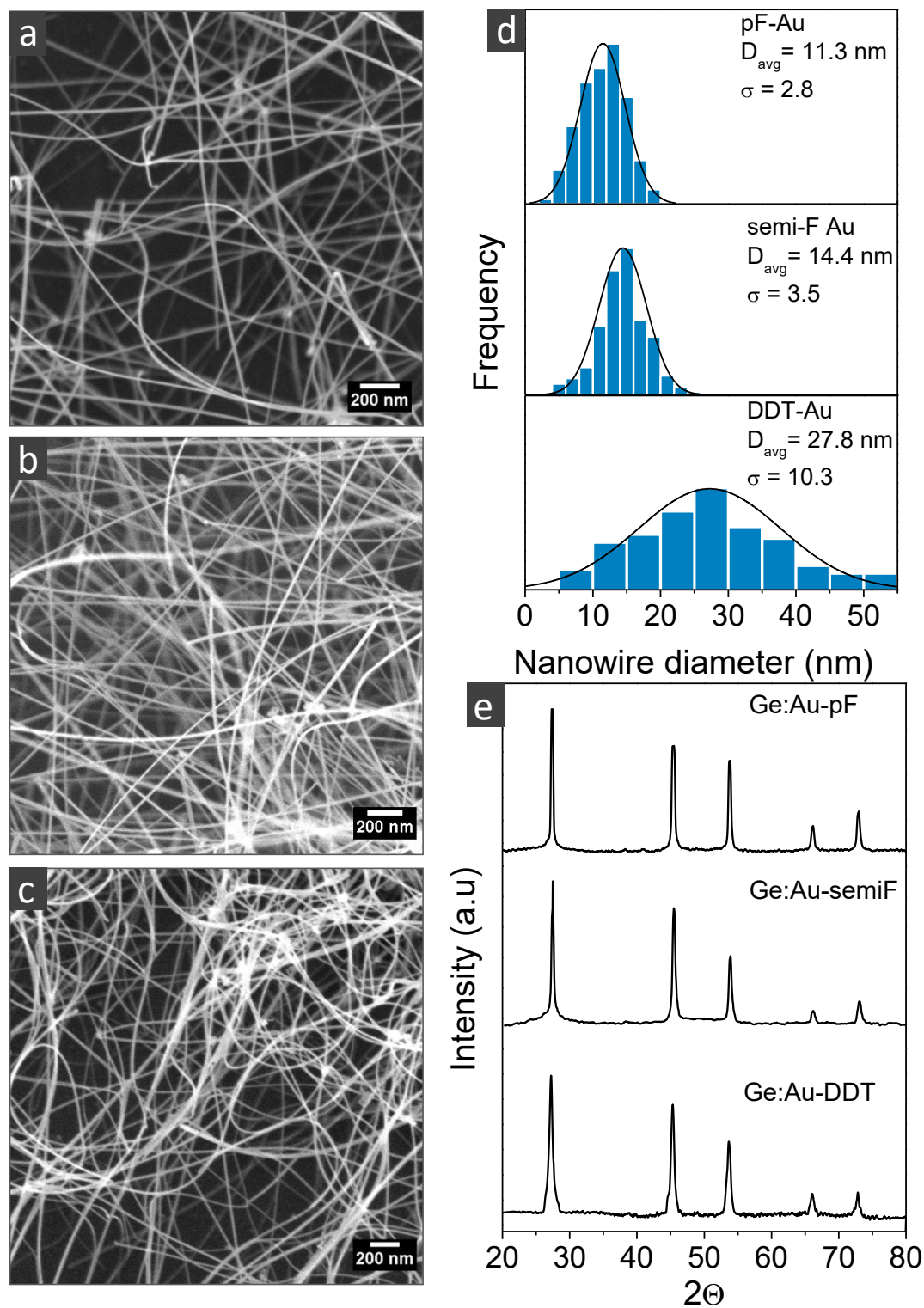


Figure 4. SEM image of Ge nanowires seeded from (a) pF-capped Au nanoparticles and (b) semi-F-capped Au nanoparticles in sc-CO₂, (c) Ge nanowires seeded from DDT-capped Au nanoparticles in sc-toluene by precursor injection, (d) histograms of the nanowire diameter distributions from the respective Au nanoparticles and (e) XRD patterns of reaction products.

Although a detailed analysis of the nanowire growth direction was not conducted, nanowires synthesized in sc-CO₂ predominantly displayed a $\langle 110 \rangle$ growth direction, as shown by the TEM images in figure 5, which is consistent with literature reports of SFLS grown Ge nanowires⁴⁴. The nature of the capping ligand and the reaction solvent did not appear to influence the nanowire growth direction.

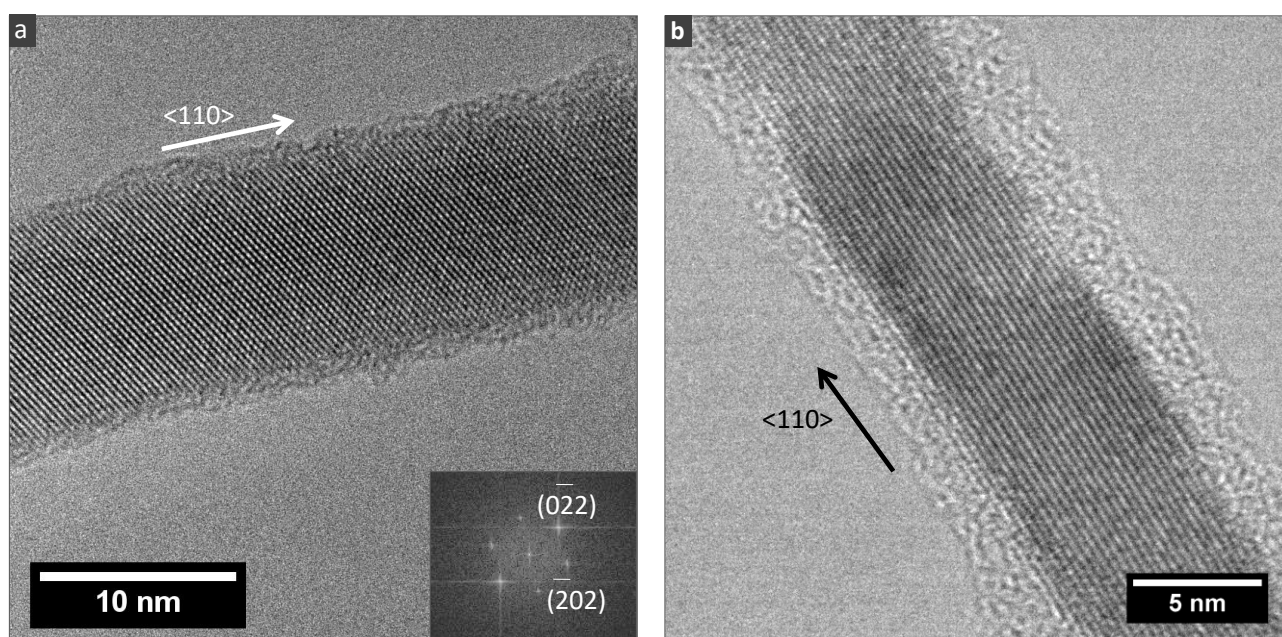


Figure 5. Ge nanowires grown in sc-CO₂, at a temperature of 380 °C and pressure of 27.6 MPa, seeded from (a) pF-capped and (b) semi-F-capped Au nanoparticles.

Table 1 summarizes the reaction conditions investigated and illustrates a clear reduction in the mean diameter of the Ge nanowires synthesized from the fluoros-capped Au nanoparticles in sc-CO₂ compared to the DDT-capped Au nanoparticles in toluene. This finding is somewhat surprising as Au attractions in CO₂ are relatively strong due to the low polarizability of the solvent and consequently, Au nanoparticles would be expected to aggregate readily in sc-CO₂ and therefore yield larger diameter nanowires. However there are considerable differences between the two synthesis conditions, *i.e.* the fluorocarbon-ligands in a sc-CO₂ environment and the hydrocarbon-ligands in a toluene solvent. The origin of the smaller mean diameter seen for Ge nanowires synthesized in the

fluorocarbon/CO₂ system was investigated as a function of the differences in (i) the solvent properties of CO₂ and toluene and the (ii) conformation and properties of the fluorocarbon versus hydrocarbon stabilising ligands.

Table 1 Summary of reaction parameters and the physical properties of the Ge nanowires obtained.

Exp	Au Nanoparticle Ligand	Solvent	Temp (°C)	D _{avg} (nm)	Std. Dev. (σ)
a	pF-Au	CO ₂	380	11.3	2.8
b	pF-Au	CO ₂ /perfluorohexane	380	12.5	2.4
c	pF-Au	CO ₂	400	16.8	3.1
d	Semi-F-Au	CO ₂	380	14.4	3.5
e	Semi-F-Au	CO ₂ /perfluorohexane	380	13.8	4.0
f	DDT-Au	Toluene	380	27.8	10.3
g	DDT-Au	Toluene	400	31.9	12.2

The electrical integrity of the as-synthesised nanowires was also tested by carrying out electrical field-effect measurements at room-temperature on individual nanowires. The synthesized nanowires were first deposited on a SiO₂ surface, thermally grown on a degenerately doped Si-substrate, which also serves as gate-electrode. Source- and drain-electrodes (300 nm wide, 80 nm high, electrode-distance 800 nm) on top of the single nanowire were defined via lithographical means^{2, 45-46}. Palladium was used as electrode-material.

In figure 6 the typical electric-field-effect transfer characteristic of a Ge nanowire is shown. A strong switching behavior with the applied gate-voltage was observed in all of the contacted nanowires of this type. This electrical response proves unambiguously that our synthesized germanium nanowires are *p*-type (hole) semiconductors since an increase in the current for negative voltages is observed. The *p*-type conduction coincides with the presence of Au during synthesis. Au

is known to be a strong electron-acceptor within germanium⁴⁷ and thus our measurements indicate that small amounts of Au-dopants might have been incorporated into the Ge nanowires during synthesis. In the inset of figure 6 the two-point current-voltage characteristics of a single nanowire is shown. The characteristic is non-linear as expected for metal/semiconductor nanowire/metal devices. Therefore, the overall electrical behaviour we have observed is characteristic for germanium nanowires as it is reported in earlier work found in literature⁴⁸⁻⁵¹.

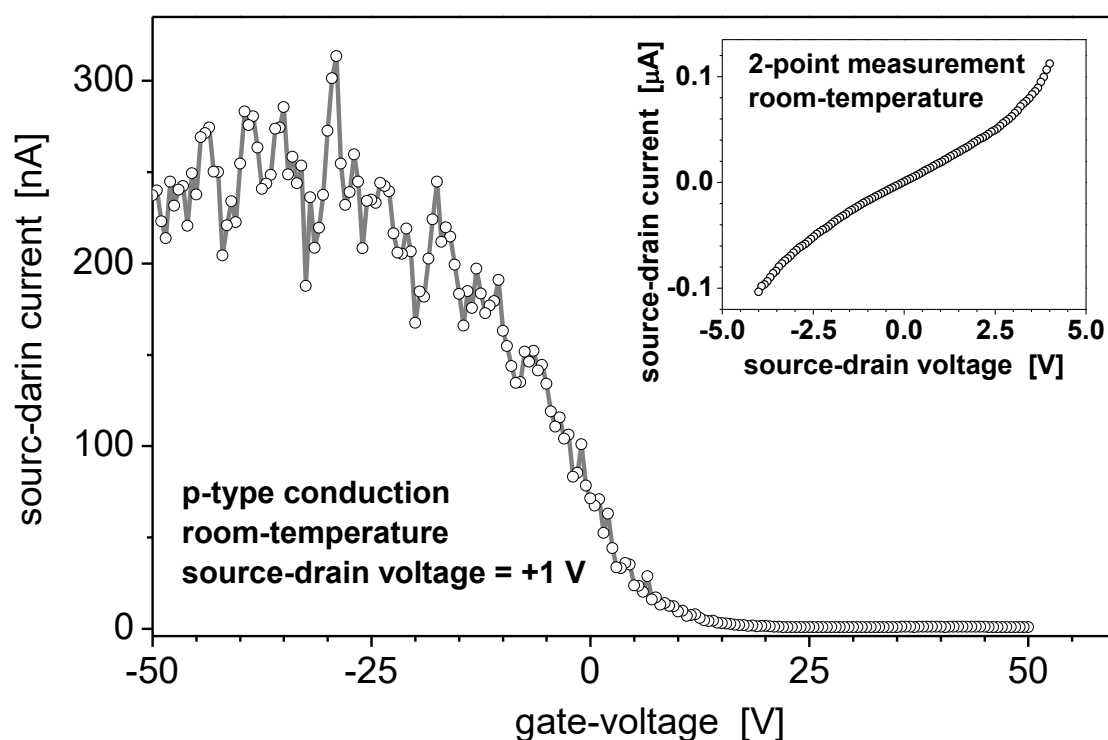


Figure 6. Electrical field-effect of a single germanium nanowire synthesised in sc-CO₂ showing typical switching behavior with gate-voltage at room temperature. The current increases with negative gate-voltage indicating that the nanowire is a hole-conductor. Inset: Typical non-linear current-voltage characteristic of a Ge nanowire contacted to metal-electrodes.

Influence of Reaction Solvent

The poor solvating ability of sc-CO₂ is well reported^{24, 52}. Hence we investigated if the smaller mean diameter Ge nanowires obtained with the fluorous-capped Au nanoparticles was simply due to the precipitation of large Au nanoparticles in the pressurized injection cell (27.6 MPa, 25 °C); resulting

in the stabilization of low concentration of small nanoparticles in CO₂ which seed the Ge nanowire growth. It should be noted that Au nanoparticles which precipitate from solution will still acts as seeds for Ge nanowire growth at the bottom of the reaction cell⁵³. An examination of the reaction product both on the Si wafer inside the reaction cell and product collected from the reaction side walls did not reveal the presence of larger diameter nanowires.

The strength of the Au van der Waals attractions across CO₂ can be estimated from the Hamaker constant using the following combining law $A_{121} \approx \left(\sqrt{A_{11}} - \sqrt{A_{22}}\right)^2$, where A_{11} is the Hamaker constant for Au across a vacuum, obtained from the literature⁵⁴. A_{22} is the Hamaker constant for CO₂ across a vacuum, which can be estimated based on Lifshitz theory⁵⁵ (equation 1):

$$A_{22} = \frac{3}{4} k_B T \left(\frac{\epsilon_2 - 1}{\epsilon_2 + 1} \right)^2 + \frac{2h\nu_e}{16\sqrt{2}} \frac{(n_2 - 1)^2}{(n_2 + 1)^{3/2}} \quad (1)$$

Where h is Plank's constant, k_B is Boltzmann's constant, T is the temperature and ν_e is the maximum electronic ultraviolet absorption frequency taken to be $3 \times 10^{15} \text{ s}^{-1}$ ⁵⁴. The density dependant dielectric constant and refractive index can be estimated from equations of state⁵⁶⁻⁵⁷. Neglecting the effects of particle size, the Hamaker constant for Au across CO₂ (A_{121}) at a temperature of 380 °C and pressure of 27.6 MPa is estimated to be 2.0 eV, while at a temperature of 25 °C and pressure of 27.6 MPa (in the injection cell) A_{121} is estimated to be 1.4 eV. Furthermore, the Hamaker constant of Ag across CO₂ at a pressure of 27.6 MPa and temperature of 80 °C, conditions known to stabilize fluorine-capped Ag nanoparticles, has been reported to be 1.5 eV⁵⁸. Estimations based on the Hamaker constants and experimental studies of fluorine-capped Ag nanoparticles indicate that the Au nanoparticles should be dispersed in sc-CO₂ at a temperature of 25 °C and a pressure of 27.6

MPa, where high CO₂ density favors good solvent conditions. Moreover, a visual inspection, through a sapphire window in the front of the injection cell, showed that all of the Au nanoparticles appeared to be well dispersed in the sc-CO₂ phase, with no precipitation of the larger particles at the bottom of the cell. However, there are also discrepancies in the literature surrounding the solubility of fluorothiolate-capped nanoparticles, for example, Shah *et al.*⁵⁹ reported that fluorinated-capped Ag nanoparticles could be dispersed in sc-CO₂ but also in acetone, an unusual solubility behaviour which Yonezawa⁶⁰ and co-workers attributed to insufficient sample purification and the presence of excess stabilizing ligand. Therefore, to improve the solvating power of CO₂ and to minimize possible Au nanoparticle precipitation, a fluorinated co-solvent, perfluorohexane, was added to CO₂ and used as the reaction solvent. Co-solvents are known to greatly enhance the solubility of solutes in CO₂⁶¹⁻⁶² and perfluorohexane, which has a critical temperature of 175 °C and critical pressure of 1.6 MPa, is miscible with CO₂ and also solubilizes the fluorinated capped Au nanoparticles⁶³. If precipitation of larger Au nanoparticles was significant for nanowires grown in sc-CO₂, the use of a co-solvent to prevent such precipitation would be expected to give rise to Ge nanowires with a larger mean diameter, compared to sc-CO₂ on its own. Ge nanowires were synthesized in a sc-CO₂/perfluorohexane (50 % v/v) solvent under the same temperature and pressure as nanowires grown in pure CO₂. Figure 7 shows SEM and TEM images of the resulting nanowires having a mean diameter (12.5 nm, $\sigma = 2.4$) and size distribution comparable to nanowires synthesized in sc-CO₂, as shown in table 1. There was however a slight increase in the amount of Ge particulates produced, most likely due to the incompatibility of the fluorinated solvent with the organo-germane precursor. The fact that Ge nanowires grown in pure CO₂ and CO₂/perfluorohexane solvents have similar diameters is suggestive that the decrease in the mean diameter of nanowires grown in sc-CO₂, when compared to toluene, is not largely attributed to the precipitation of large Au nanoparticles in the reaction cell.

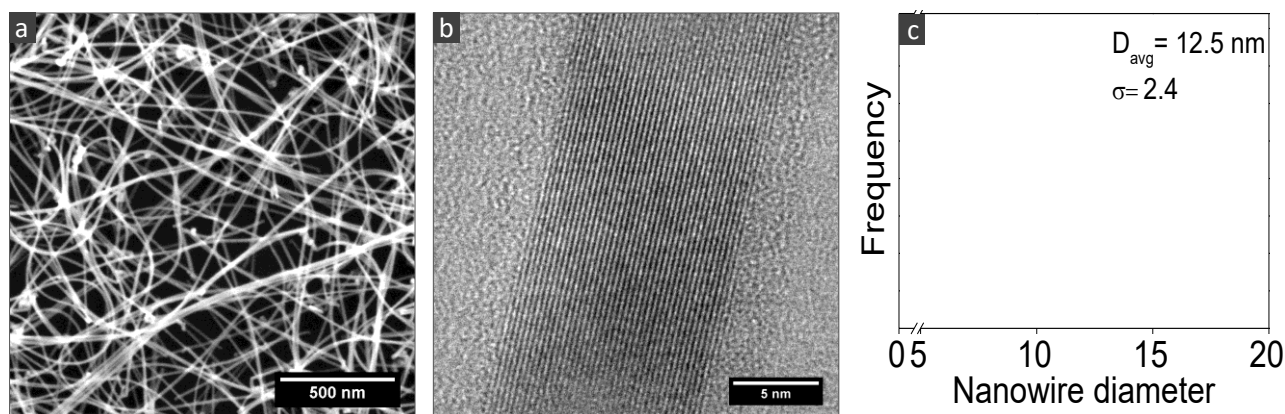


Figure 7. (a) SEM image, (b) TEM image and (c) size distribution histogram of Ge nanowires synthesized in sc-CO₂/perfluorohexane at a temperature of 380 °C and a pressure of 27.6 MPa.

In VLS growth the mean nanowire diameter is determined by the dimensions of the saturated Au:Ge eutectic droplet from which they nucleate¹³. A large variation in the distribution of nanowire diameters in any given sample usually results from the agglomeration of the Au nanoparticles, or Au-Ge liquid alloy droplets, prior to nanowire growth. There are two important factors which affect nanowire growth from the saturated Au seed. Firstly, the diffusion rate of the Ge precursor to the Au nanoparticle determines how fast saturation of the catalyst particle occurs, with faster diffusion rates resulting in smaller diameter nanowires¹². Korgel *et al.*¹⁶ reported that alkyl-germane precursors have slower decomposition kinetics compared to aryl-germanes, leading to longer seed saturation times and consequently broader diameter distributions for nanowires grown in SCFs. While the decomposition kinetics of aryl silanes has been shown to be influenced by the reaction solvent⁶⁴, aryl germane decomposition appears to be much less dependent on solvent properties, which can be attributed to the higher reactivity of aryl-germanes⁶⁵. In fact DPG has proved a versatile precursor for Ge nanowire synthesis in a wide range of solvents including CO₂, hexane, toluene and high boiling solvents such as squalene, trioctylamine and triphenylphosphine^{14, 44, 66-67}. In our experiments it is unlikely that the decomposition kinetics of the DPG would differ considerably in sc-CO₂ and sc-toluene under the same reaction conditions of temperature and pressure; there is no apparent functionality of either solvent that could significantly affect the stability of the

intermediates. There is little evidence to suggest that the smaller mean diameter of nanowires grown in sc-CO₂ is attributable to the faster decomposition of the Ge precursor in CO₂ compared to toluene.

The second contributor to broadening of the nanowire diameter distribution in VLS growth is the degree of aggregation of the catalyst nanoparticles. To prevent colloidal aggregation the van der Waals forces of attractions between the Au cores must be mediated by the steric repulsion provided by the capping ligands. At high solvent density the capping ligands are well solvated, as the presence of solvent in between the ligands screens the intra-chain attractions. As the solvent density decreases, solvent molecules move away from the ligands in order to gain entropy and solvent quality diminishes. Under these poor solvent conditions the chains contract and no longer provide adequate steric repulsion to overcome the attractive core interactions, resulting in nanoparticle aggregation.

When the Au nanoparticles were heated to the reaction temperature in the absence of DPG, the nanoparticles underwent significant aggregation (> 50 nm) regardless of the nature of the capping ligand or solvent. One noticeable difference was that the diameters of the aggregated fluorinated nanoparticles were more monodisperse than the aggregated DDT-capped nanoparticles (see supporting information, figure S1, for TEM and size distribution analysis). A similar observation was made by Korgel and co-workers¹⁶ for Ge nanowire growth in sc-cyclohexane, who reported that without the onset of nanowire growth, the catalyst particles underwent far greater aggregation. Colloidal stability of fluorous-capped Au nanoparticle in sc-CO₂ would be expected to differ from hydrocarbon-capped Au nanoparticles in sc-toluene due to differences in solvent properties and ligand characteristics. Therefore, the role of the capping ligands as a function of conformation and stability at high temperatures was investigated.

Influence of Ligand Conformation and Nanoparticle Stability

The greater the degree of nanoparticle aggregation the larger and more polydisperse are the resulting nanowires from which they nucleate. Consequently, a plausible mechanism for the smaller and narrower diameter distributions obtained for the fluorocarbon/CO₂ system may stem from reduced nanoparticle aggregation relative to those in the hydrocarbon/toluene environment. TGA analysis of the Au nanoparticles in figure 2(b) shows that the semi-F ligands begin to desorb at a higher temperature (~220 °C) compared to the DDT ligands, reflecting the higher boiling point of the ligand. Desorption of the capping ligands results in partially protected nanoparticles which are extremely susceptible to aggregation as the loss of the ligands gives rise to a loss of steric repulsion between the nanoparticles⁵⁸. TGA profiles of the pF-capped and DDT-capped Au nanoparticles show that while both ligands begin to desorb at similar temperatures (~180 °C), the fluorinated ligands desorb over a wider temperature range, most likely due to the lower volatility of the fluororous ligands. The length of the capping ligands also influences nanoparticle aggregation with longer ligand lengths providing a greater interparticle separation distance and improved steric stabilization relative to shorter ligands⁵⁹. The length of a DDT ligand is 18 Å, which is shorter compared to the fluororous ligands, ~21 Å for pF, and ~22 Å for semi-F. Fluorocarbons and hydrocarbons also display differences in chain conformation⁶⁸. Unlike hydrocarbon chains which adopt a planar zig-zag conformation, fluorocarbons assume a helical structure due to the steric repulsion between the bulky fluorine atoms. These steric constraints make fluorocarbons more rigid compared to their hydrocarbon analogues⁶⁹. A combination of slower capping ligand desorption, longer ligand lengths and greater rigidity of the fluorocarbon chains would reduce nanoparticle aggregation, leading to smaller diameter nanowires.

Interactions between the stabilising ligands and the solvent affects ligand conformation and Monte Carlo simulations have shown that ligand conformation plays an important role in colloidal interactions in SCFs⁷⁰⁻⁷³. Chain conformation strongly depends on solvent quality and solvents are

generally classified as ‘good’ solvents in which ligands assume a coil-like conformation and extend out into the solvent, or a ‘poor’ solvent in which the ligands adopt a compact globular structure. Luna-Bárcenas *et al.*⁷⁰ found that as solvent density is decreased, a chain in a SCF collapses from an extended to a closed conformation at the coil-to-globule transition density (C-GTD). Figure 8 (taken from reference 49) illustrates the variation of the C-GTD as a function of the reduced temperature (T_r), where $T_r = T/T_c$. As the temperature increases the reduced density causes the chain attractions to dominate and the ligands collapse near the well known lower critical solution temperature (LCST)⁷⁴. However, as the temperature is increased further the chains become extended again. This chain expansion is attributed to the attractive energies becoming less important relative to the thermal energy of the system as shown by the Flory parameter χ (equation 2)⁷¹:

$$\chi \approx \frac{\varepsilon_{11} + \varepsilon_{22} - 2\varepsilon_{12}}{k_B T} \quad (2)$$

where ε_{11} and ε_{22} are the strength of the ligand and solvent interactions, respectively. The solvent isobar shown in figure 8 represents a reduced pressure (P_r) of 3.7, where $P_r = P/P_c$, and is the reaction pressure used for the Ge nanowire synthesis in sc-CO₂ in our study. According to simulations, at a $P_r = 3.7$, chain collapse will occur at a $T_r = 1.37$ and the chain will re-expand on further heating at a $T_r > 1.65$, as the attractive chain interactions become less pronounced at higher temperatures. Simulations predict that under the synthesis conditions of $P_r = 3.7$ and $T_r = 2.2$, the ligands will have an extended conformation even though solvent density is low; thereby allowing for some degree of steric stabilization. Neutron reflectivity⁷⁵ and SANS⁷⁶ measurements have shown oligomer solvation in CO₂ to improve at higher temperatures for a given solvent density. Korgel *et al.*⁷⁷ provided experimental support for colloidal stabilization in low density sc-CO₂ reporting that octanol was effective in stabilising 10 nm Ge nanocrystals synthesized in sc-CO₂ at a $T_r = 2.5$.

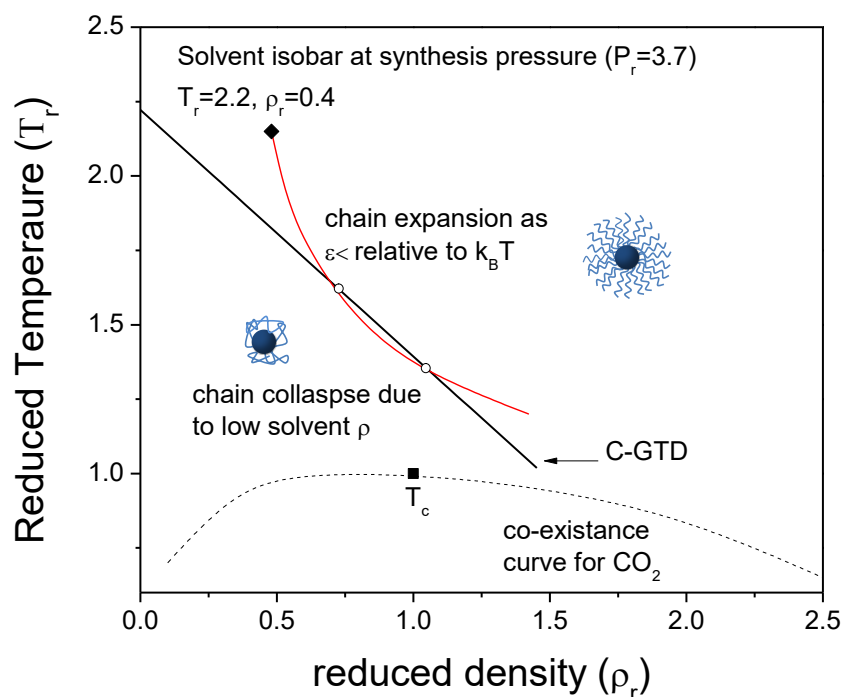


Figure 8. Coil-to-globule transition density (C-GTD) as a function of temperature. T_c represents the critical point for CO_2 . Data reproduced from reference 49.

When the fluororous-capped Au nanoparticles and DPG are heated to the reaction temperature in the absence of CO_2 , large aggregated particles are produced, illustrating the importance of CO_2 in providing some degree of solvation to the nanoparticles. It must be noted that the Au nanoparticles still undergo aggregation, the initial mean diameter of the nanoparticles is ~ 2.2 nm, but the fluorinated ligands in sc- CO_2 may provide a greater degree of stabilization relative to the hydrocarbon ligands in sc-toluene, and hence the resulting mean diameter of the nanowires grown in sc- CO_2 are smaller than those grown in sc-toluene. While computer simulations do not adequately describe the phase behaviour of oligomers in supercritical organic solvents, these studies provide insights into the fundamental effects of ligand and solvent interactions. Luna-Bárcenas and co-workers⁷² defined a conformational parameter (ψ) to describe the universal effects of solvent-ligand energetic interactions and size ratio, where $\psi < 1$ constitutes a good solvent system (equation 3):

$$\Psi = \frac{(\varepsilon_{11} / \varepsilon_{22})}{(\sigma_{11} / \sigma_{22})^3} \quad (3)$$

ε_{11} and ε_{22} represent the ligand-ligand and solvent-solvent energetic interactions, σ_{11} and σ_{22} represent the ligand and solvent size, respectively. From equation 3, an increase in the chain interactions relative to solvent interactions favours chain collapse as the solvent is less effective at solvating the ligands and ψ increases. The high electronegativity and low polarizability of fluorine results in very weak ligand interactions, compared to hydrocarbon chains⁷⁸. In sc-toluene, the stronger chain attractions may render the chains less effective in mediating core-attractions.

Conclusions

Fluorous-capped Au nanoparticles provide an alternative solvent for the SCF synthesis of Ge nanowires as the fluorinated ligands allows for the dispersibility of the catalyst in sc-CO₂. Ge nanowires synthesized from fluorous-capped Au nanoparticles have smaller mean diameters, with narrower size distributions, compared to DDT-capped nanoparticles synthesized in sc-toluene. The smaller mean diameter of nanowires grown in sc-CO₂ may be attributed to the greater degree of Au nanoparticle stabilization experienced by the fluorinated-capped nanoparticles, due to a combination of longer ligand length, increased ligand rigidity and better solvation at high temperatures; owing to weaker chain interactions compared to hydrocarbon ligands. Furthermore, the experimental results support MC simulation predictions that colloidal stabilization in sc-CO₂ is possible even in low solvent density. The electrical behavior of the Ge nanowires is characteristic to what has previously been reported in the literature for Au-seeded semiconductor nanowires.

Acknowledgements

We acknowledge financial supported by the Irish Research Council for Science and Engineering Technology (IRCSET) and Science Foundation Ireland (Grant 08/CE/I1432). This research was also enabled by the Higher Education Authority Program for Research in Third Level Institutions (2007-2011) via the INSPIRE programme.

References

1. Xiang, J.; Lu, W.; Hu, Y.; Wu, Y.; Yan, H.; Lieber, C. M., *Nature* **2006**, *441*, 489.
2. Li, Y.; Qian, F.; Xiang, J.; Lieber, C. M., *Mater. Today* **2006**, *9* (10), 18.
3. Hsin, C.-L.; Mai, W.; Gu, Y.; Huang, C.-T.; Lui, Y.; Chen, L.-J.; Wang, Z.-L., *Adv. Mater.* **2008**, *20* (20), 3919.
4. Huang, Y.; Duan, X.; Cui, Y.; Lauhon, L. J.; Kim, K.-H.; Lieber, C. M., *Science* **2001**, *294* (9), 1313.
5. Huang, Y.; Lieber, C. M., *Pure Appl. Chem.* **2004**, *76* (12), 2051.
6. Cui, Y.; Lieber, C. M., *Science* **2001**, *291* (5505), 851.
7. Maeda, Y.; Tsukamoto, N.; Yazawa, Y., *Appl. Phys. Lett.* **1991**, *59*, 3168.
8. Lew, K. K.; Reuther, C.; Carim, A. H.; Redwing, J. M.; Martin, B. R., *J. Vac. Sci. Technol. B* **2002**, *20* (1), 389.
9. Jagannathan, H.; Deal, M.; Nishi, Y.; Kim, H. C.; Freer, E. M.; Sundstrom, L.; Topuria, T.; Rice, P. M., *J. Vac. Sci. Technol. B* **2006**, *24* (5), 2220.
10. Sun, X. H.; Didychuk, C.; Sham, T. K.; Wong, N. B., *Nanotechnology* **2006**, *17*, 2925.
11. Song, M. S.; Jung, J. H.; Kim, Y.; Wang, Y.; Zou, J.; Joyce, H. J.; Gao, Q.; Tan, H. H.; Jagadish, C., *Nanotechnology* **2008**, *19*, 125602.
12. Wang, D. W.; Tu, R.; Zhang, L.; Dai, H. J., *Angew. Chem. Int. Ed.* **2005**, *44* (19), 2925.
13. Wu, Y.; Yang, P., *J. Am. Chem. Soc.* **2001**, *123*, 3165.

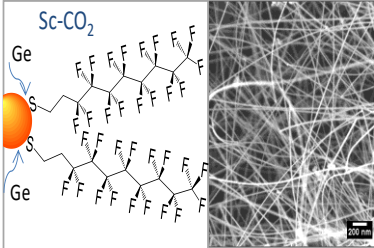
14. Chockla, A. M.; Korgel, B. A., *J. Mater. Chem.* **2009**, *19*, 996.
15. Woodruff, J. H.; Ratchford, J. B.; Goldthorpe, I. A.; McIntyre, P. C.; Chidsey, C. E. D., *Nano Lett.* **2007**, *7* (6), 1637.
16. Hanrath, T.; Korgel, B. A., *J. Am. Chem. Soc.* **2002**, *124* (7), 1424.
17. Hanrath, T.; Korgel, B. A., *Adv. Mater.* **2003**, *15* (5), 437.
18. Lu, X.; Fanfair, D. D.; Johnston, K. P.; Korgel, B. A., *J. Am. Chem. Soc.* **2005**, *127*, 15718.
19. Tuan, H.-Y.; Lee, D. C.; Hanrath, T.; Korgel, B. A., *Chem. Mater.* **2005**, *17*, 5705.
20. Tuan, H.-Y.; Lee, D. C.; Korgel, B. A., *Angew. Chem. Int. Ed.* **2006**, *45*, 5184.
21. Jessop, P. G.; Leitner, W., *Wiley-VCH* **1999**.
22. O'Neill, M. L.; Fang, Q. C. M.; Johnston, K. P., *Ind. Eng. Chem. Res.* **1998**, *37*, 3067.
23. Raveedran, P.; Ikushima, Y.; Wallen, S. L., *Acc. Chem. Res.* **2005**, *38*, 478.
24. Consani, K. A.; Smith, R. D., *J. Supercrit. Fluids* **1990**, *3*, 51.
25. Eastoe, J.; Dupont, A.; Steytler, D. C., *J. Colloid Interf. Sci.* **2003**, *8*, 267.
26. Harrison, K.; Goveas, J.; Johnston, K. P.; Orear, E. A., *Langmuir* **1994**, *10* (10), 3536.
27. Shah, P.; Holmes, J. D.; Doty, R. C.; Johnston, K. P.; Korgel, B. A., *J. Am. Chem. Soc.* **2000**, *122*, 4245.
28. Kameo, A.; Yoshimura, T.; Esumi, K., *Colloid Surface A* **2003**, *215*, 181.
29. Dardin, A.; DeSimone, J. M.; Samulski, E. T., *J. Phys. Chem. B* **1998**, *102*, 1775.
30. Yonker, C., *J. Phys. Chem. A* **2000**, *104*, 685.
31. Yonker, C.; Palmer, B., *J. Phys. Chem. A* **2001**, *105*, 308.
32. Wallen, S. L.; Raveedran, P., *J. Phys. Chem. B* **2003**, *107*, 1473.
33. Naud, C.; Blancou, H.; Commeyras, A., *J. Fluorine Chem.* **2000**, *104*, 173.
34. Troughton, E. B.; Bain, C. D.; Whitesides, G. M., *Langmuir* **1988**, *4*, 365.
35. Brust, M.; Walker, M.; Bethell, D.; Schiffrin, J.; Whyman, R., *J. Chem. Soc., Chem. Commun.* **1994**, 801.
36. Dass, A.; Guo, R.; Tracy, J. B.; Balasubramanian, R.; Douglas, A. D.; Murray, R. W., *Langmuir* **2008**, *24* (1), 310.

37. Chlistunoff, J.; Ziegler, K. J.; Lasdon, L.; Johnston, K. P., *J. Phys. Chem. A* **1999**, *103*, 1678.
38. Tsao, M.-W.; Hoffmann, C. L.; Rabolt, J. F., *Langmuir* **1997**, *13*, 4317.
39. Yang, Y. W.; Fan, L. J., *Langmuir* **2002**, *18* (4), 1157.
40. Castner, D. G.; Hinds, K.; Grainger, D. W., *Langmuir* **1996**, *12* (21), 5083.
41. Joseph, Y.; Besnard, I.; Rosenberger, M.; Guse, B.; Nothofer, H. G.; Wessels, J. M.; Wild, U.; Knop-Gericke, A.; Su, D. S.; Schlogl, R.; Yasuda, A.; Vossmeier, T., *J. Phys. Chem. B* **2003**, *107* (30), 7406.
42. Watts, J. F.; Wolstenholme, J., *An Introduction to Surface Analysis by XPS and AES*. John Wiley & Sons Ltd.: West Sussex, England, 2003.
43. Dass, A.; Guo, R.; Tracy, J. B.; Balasubramanian, R.; Douglas, A. D.; Murray, R. W., *Langmuir* **2008**, *24* (1), 310.
44. Hanrath, T.; Korgel, B. A., *Small* **2005**, *1* (7), 717.
45. Madon, M. J., *Fundamentals of Microfabrication: The Science of Miniaturization*. 2nd Ed. ed.; CRC Press: University of California, Irvine, USA, 2002.
46. Lu, W.; Lieber, C. M., *J. Phys. D-Appl. Phys.* **2006**, *39* (21), R387.
47. Dunlap, W. C., *Phys. Rev.* **1955**, *97* (3), 614.
48. Hanrath, T.; Korgel, B. A., *Proc. IMechE, Part N: J. Nanoengineering and Nanosystems* **2004**, *218* (1), 25.
49. Greytak, A. B.; Lauhon, L. J.; Gudiksen, M. S.; Lieber, C. M., *Appl. Phys. Lett.* **2004**, *84* (21), 4176.
50. Wang, D. W.; Wang, Q.; Javey, A.; Tu, R.; Dai, H. J.; Kim, H.; McIntyre, P. C.; Krishnamohan, T.; Saraswat, K. C., *Appl. Phys. Lett.* **2003**, *83* (12), 2432.
51. Wang, D.; Dai, H., *Applied Physics A* **2006**, *85*, 217.
52. Gupta, R. B.; Shim, J.-J., *Solubility in Supercritical Carbon Dioxide*. CRC Press: Boca Raton, FL, 2007.
53. van der Meulen, M. I.; Petkov, N.; Morris, M. A.; Kazakova, O.; Han, X. H.; Wang, K. L.; Jacob, A. P.; Holmes, J. D., *Nano Lett.* **2009**, *9* (1), 50.

54. Israelachvili, J., *Intermolecular and Surface Forces*. Academic Press: London, UK, 1991; Vol. 2nd ed.
55. Hamaker, H. C., *Physica* **1937**, *4*, 1058.
56. Keyes, F.; Kirkwood, J. G., *Phys. Rev.* **1930**, *36*, 754.
57. Lewis, J. E.; Biswas, R.; Robinson, A. G.; Maroncelli, M., *J. Phys. Chem. B* **2001**, *105*, 3306.
58. Shah, P. S.; Husain, S.; Johnston, K. P.; Korgel, B. A., *J. Phys. Chem. B* **2002**, *106*, 12178.
59. Shah, P.; Husain, S.; Johnston, K. P.; Korgel, B. A., *J. Phys. Chem. B* **2001**, *105*, 9433.
60. Yonezawa, T.; Onoue, S.; Kimizuka, N., *Langmuir* **2001**, *17*, 2291.
61. Dobbs, J. M.; Wong, J. M.; Johnston, K. P., *J. Chem. Eng. Data* **1986**, *31*, 303.
62. Ke, J.; Mao, C.; Zhong, M. H.; Han, B. X.; Yan, H. K., *J. Supercrit. Fluids* **1996**, *9* (2), 82.
63. Dunlap, R. D.; Murphy, C. J.; Bedford, R. G., *J. Am. Chem. Soc.* **1958**, *80* (1), 83.
64. Tuan, H.-Y.; Korgel, B. A., *Chem. Mater.* **2008**, *20*, 1239.
65. Smirnov, V. N., *Kinetics and Catalysis* **2007**, *48* (5), 615.
66. Kazakova, O.; Kulkarni, J. S.; Holmes, J. D.; Demokritov, S. O., *Phys. Rev. B* **2005**, *72* (9).
67. Ryan, K. M.; Erts, D.; Olin, H.; Morris, M. A.; Holmes, J. D., *J. Am. Chem. Soc.* **2003**, *125* (20), 6284.
68. Barriet, D.; Randall Lee, T., *Colloid Interf. Sci.* **2003**, *8*, 236.
69. Eaton, D. F.; Smart, B. E., *J. Am. Chem. Soc.* **1990**, *112* (7), 2821.
70. Luna-Barcenas, G.; Gromov, D. G.; Meredith, J. C.; Sanchez, I. C.; de Pablo, J. J.; Johnston, K. P., *Chem. Phys. Lett.* **1997**, *278*, 302.
71. Luna-Barcenas, G.; Meredith, J. C.; Sanche, I. C.; Johnston, K. P., *J. Chem. Phys.* **1997**, *107* (24), 10782.
72. Ortiz-Estrada, C. H.; Luna-Barcenas, G.; Alvarado, F. J.; Gonzalez-Alatorre, G.; Sanchez, I. C.; Castillo-Tejas, J.; Manero-Brito, M.; Ramirez, N. F.; Garcia, S. R. V., *Macromol. Symp.* **2009**, *283*, 250.

73. Gromov, D. G.; de Pablo, J. J.; Luna-Barcenas, G.; Sanchez, I. C.; Johnston, K. P., *J. Chem. Phys.* **1998**, *108* (11), 4674.
74. Meredith, J. C.; Sanchez, I. C.; Johnston, K. P.; de Pablo, J. J., *J. Chem. Phys.* **1998**, *109* (15), 6424.
75. Sirard, S. M.; Gupta, R., T. P.; Watkins, J. J.; Green, P. F.; Johnston, K. P., *Macromolecules* **2003**, *36*, 3365.
76. Melnichenko, Y. B.; Kiran, E.; Heath, K. D.; Salaniwal, S.; Cochran, H. D.; Stamm, M.; van Hook, W. A.; Wignall, G. D., *Crystallogr.* **2000**, *33*, 682.
77. Lu, X.; Korgel, B. A.; Johnston, K. P., *Nanotechnology* **2005**, *16*, 389.
78. Drummond, C. J.; Georgaklis, G.; Chan, D. Y. C., *Langmuir* **1996**, *12* (11), 2617.

Table of Contents

Gillian Collins, Maria Kolečnik, Vojislav Krstić and Justin D. Holmes	Ge nanowires seeded from Au nanoparticles capped with fluorothiolate ligands were synthesized in supercritical carbon dioxide, resulting in small diameter (< 20 nm) nanowires with a relatively narrow size distribution.	
---	--	--